Research Square

Preprints are preliminary reports that have not undergone peer review.
They should not be considered conclusive, used to inform clinical practice,
or referenced by the media as validated information.

Suxiao Jiuxin Pills Attenuate Myocardial Ischemia Injury through Multi-Component Synergy and Ligustilide-Mediated AKT/GSK3β/HIF-1α Pathway Activation

yue weng
Tianjin University of Traditional Chinese Medicine
Xinyu he
Tianjin University of Traditional Chinese Medicine
Peishuang yu
Tianjin University of Traditional Chinese Medicine
Yujie gong
Tianjin University of Traditional Chinese Medicine
Xueke liu
Tianjin University of Traditional Chinese Medicine
Yanyan xu
Tianjin University of Traditional Chinese Medicine
shenshen yang
yss2099@tjutcm.edu.cn
Tianjin University of Traditional Chinese Medicine

Research Article

Keywords: Suxiao Jiuxin Pills, Myocardial Infarction, Ligustilide, Material Basis of Medicinal Efficacy, AKT/GSK3β/HIF-1α

Posted Date: September 29th, 2026

DOI: https://doi.org/10.21203/rs.3.rs-10508035/v1

License: This work is licensed under a Creative Commons Attribution 4.0 International License.
Read Full License

Additional Declarations: No competing interests reported.

Abstract

Myocardial infarction (MI), resulting from acute occlusion of the coronary artery, induces myocardial ischemia, hypoxia, and necrosis, and remains a leading cause of morbidity and mortality worldwide. Suxiao Jiuxin Pills (SJP), a widely used proprietary Chinese medicine for coronary heart disease and angina pectoris, have yet to be fully elucidated regarding their cardioprotective efficacy and underlying mechanisms against AMI. In the present study, an AMI mouse model was generated via permanent ligation of the left anterior descending (LAD) artery. Mice were randomly assigned to five groups: sham-operated, model, low-dose SJP (78 mg/kg), high-dose SJP (156 mg/kg), and captopril (positive control). Following 7 consecutive days of intragastric gavage, cardiac function, serum biomarkers of myocardial injury, and infarct size were systematically evaluated. Concurrently, an oxygen-glucose deprivation (OGD) model was established in H9c2 cardiomyocytes to investigate the protective actions of four major SJP constituents—borneol(BOR), ferulic acid(FA), ligustilide (LIG), and senkyunolide A(SEA). In vivo, SJP treatment significantly preserved cardiac performance, diminished circulating levels of Creatine kinase MB (CK-MB), cardiac troponin T (cTnT), and Lactate dehydrogenase (LDH), attenuated histopathological damage and interstitial fibrosis, and markedly reduced the extent of myocardial infarction. In vitro, all four compounds concentration-dependently improved cell survival and counteracted oxidative injury. Mechanistic exploration revealed that LIG, in particular, preserved mitochondrial membrane potential through activation of the AKT/GSK3β signaling cascade, concomitant with suppression of HIF-1α overexpression. Collectively, these findings demonstrate that SJP confers substantial protection against ischemic/hypoxic myocardial injury, an effect attributable, at least in part, to LIG-mediated regulation of the AKT/GSK3β/HIF-1α axis and the consequent stabilization of mitochondrial homeostasis.

1. INTRODUCTION

Myocardial infarction (MI) is a severe cardiovascular disease caused by acute coronary occlusion. Myocardial infarction, characterised by necrosis of the heart muscle, is associated with a high mortality and disability rate, and thus poses a significant threat to the physical and mental health of middle-aged and elderly populations.[1] The pathological feature underpinning this condition is insufficient blood and oxygen supply to the heart, resulting in cardiac dysfunction and metabolic disorders. These, in turn, can induce arrhythmia, myocardial infarction, and other complications, and even sudden death in severe cases.[2] The occurrence of myocardial ischemia in cardiomyocytes instigates a sequence of events including hypoxic stress, mitochondrial dysfunction, excessive oxidative stress, and an inflammatory cascade, culminating in irreversible myocardial injury within a short period of time.[3] Consequently, early intervention and myocardial protection are of critical clinical significance for improving the prognosis of patients with this disease.[4]

Suxiao Jiuxin Pills (SJP) is a classic traditional Chinese medicine compound. It is primarily composed of Ligusticum chuanxiong and borneol (BOR). [5] The medication has the advantages of rapid onset, mild medicinal properties, high cost-effectiveness, and good safety. It is clinically used for emergency and routine treatment of myocardial ischemia, coronary heart disease, and angina pectoris, with stable and

definite efficacy. [6] Modern pharmacological studies have confirmed that SJP can dilate coronary arteries, improve myocardial microcirculation, inhibit platelet aggregation, effectively antagonise oxidative stress, and reduce myocardial inflammatory injury. Thus, it ameliorates the pathological state of myocardial ischemia through multiple pathways [7]. Its pharmacodynamic material basis mainly includes phthalides, such as ligustilide (LIG), senkyunolide A (SEA), and organic acids, such as ferulic acid (FA) from Ligusticum chuanxiong. Each active component exerts cardiotonic effects.It has been demonstrated that the effects of the substance in question are protective and act in a synergistic manner.[8]

Among the various active components of SJP, LIG is the key monomer responsible for cardioprotection and a subject of considerable interest in the current cardiovascular pharmacological research. As demonstrated by previous studies, LIG has been shown to possess significant anti-inflammatory, antioxidant, anti-apoptotic, and tissue-protective properties. The substance has been demonstrated to exert a protective effect on the nervous system,[9] in addition to exhibiting remarkable pharmacological value within the cardiovascular system. This component has been demonstrated to effectively scavenge excess oxygen-free radicals in cardiomyocytes. In addition, it has been shown to alleviate oxidative stress injury, inhibit local myocardial inflammatory responses and myocardial fibrosis, block the development of pathological myocardial hypertrophy and protect ischemic myocardial tissue from multiple dimensions.[10–12] Meanwhile, LIG has been shown to target and repair mitochondrial structural and functional damage caused by myocardial ischemia. Furthermore, it has been demonstrated to stabilise mitochondrial membrane potential, maintain normal energy synthesis and metabolism in cardiomyocytes, inhibit hypoxia-induced cardiomyocyte apoptosis, ensure cardiomyocyte survival and effectively delay the pathological progression of myocardial ischemia.[13]

In this study, the overall efficacy of SJP was comprehensively evaluated in a mouse acute MI model. Subsequently, the main absorbed active components, including BOR, FA, LIG, and SEA, were investigated in an oxygen-glucose deprivation (OGD) model of H9c2 cardiomyocytes.[14] Finally, the focus was on LIG and its mechanism of action was investigated from the perspectives of mitochondrial function and the AKT/GSK3β/HIF-1α pathway. Although this pathway has been previously implicated in cellular hypoxic responses,[15] its role in mediating the cardioprotective effects of specific active components derived from traditional Chinese medicine—particularly ligustilide from SJP—remains poorly defined. The objective of this study was to ascertain whether LIG exerts a protective effect on the heart against ischaemic injury by modulating the AKT/GSK3β/HIF-1α pathway and preserving mitochondrial function.

2. MATERIALS AND METHODS

2.1 Materials

SJP (Tianjin Darentang) and captopril (Changzhou Pharmaceutical Factory) were commercially available. SJP was suspended in 0.5% sodium carboxymethyl cellulose (CMC-Na). Mouse doses were converted from the maximum adult clinical dose based on body surface area: low-dose 78 mg/kg (1-fold

clinical equivalent dose) and high-dose 156 mg/kg (2-fold clinical equivalent dose). Tribromoethanol stock and working solutions were prepared using standard methods. BOR, FA, LIG, and SEA standards were purchased from Shanghai Yuanye Biotechnology, and 200 mM stock solutions were prepared in dimethyl sulfoxide (DMSO). Creatine kinase-MB (CK-MB) and cardiac troponin T (cTnT) assay kits were obtained from Nanjing Jiancheng and Wuhan Geneme, respectively. CCK-8, reactive oxygen species (ROS), and mitochondrial membrane potential (JC-1) kits were purchased from Solarbio. Lactate dehydrogenase (LDH), superoxide dismutase (SOD), and malondialdehyde (MDA) kits were supplied by Nanjing Jiancheng.

2.2 Animal Experiments

Establishment of Mouse Acute Myocardial Infarction (MI) Model by Left Anterior Descending Coronary Artery Ligation. Fifty mice were subjected to ligation to establish the acute MI model, and 32 mice were successfully modeled. These 32 mice were randomly divided into 4 groups: MI model group (n = 8), low-dose SJP group (SJP-L, n = 8), high-dose SJP group (SJP-H, n = 8), and positive drug captopril group (n = 8). An additional 8 mice underwent the same surgical procedure without coronary ligation and served as the sham-operated group (Sham, n = 8). Mice in the SJP-L and SJP-H groups were administered SJP by intragastric gavage at doses of 78 and 156 mg/kg, corresponding to 1- and 2-fold of the clinical equivalent dose, respectively. The positive control group received captopril at 20 mg/kg. The Sham and MI groups were administered an equal volume of vehicle. All treatments were administered once daily for 7 consecutive days. All animal procedures were approved by the Animal Ethics Committee of Tianjin University of Traditional Chinese Medicine (Approval No. TCM-LAEC2024080z1633). Due to unexpected mortality during the experiment, 6 mice per group with full data were included in the final statistical analysis.

2.3 General Observation and Cardiac Index

General conditions of all mice were observed daily throughout the experimental period. Body weight of each mouse was recorded before daily intragastric administration, and changes in body weight, food and water intake, mental status, and hair luster were monitored. After harvesting, the heart tissue samples were accurately weighed. The cardiac index (heart weight/body weight, HW/BW) was calculated as follows: Cardiac index (%) = [Heart weight (g) / Body weight (g)] × 100

2.4 Echocardiographic Examination

After the last administration, all mice were fasted for 12 hours with free access to water. Anesthesia was induced with isoflurane, and M-mode echocardiography was performed at the papillary muscle level. The following parameters were measured: left ventricular end-diastolic diameter (LVIDd), left ventricular end-systolic diameter (LVIDs), ejection fraction (EF), and fractional shortening (FS).

2.5 Histopathology and TTC Staining

Heart tissues were fixed in 4% paraformaldehyde, dehydrated, embedded, and sectioned. Hematoxylin and Eosin (H&E) staining was performed to observe myocardial structure, and Masson staining was

used to assess fibrosis. Frozen heart sections were subjected to 2,3,5-triphenyltetrazolium chloride (TTC) staining, and the myocardial infarct size was calculated.

2.6 Serum Biochemical Assays

LDH content was determined by the microplate method following the instructions of the LDH assay kit. Following the manufacturer's protocol of the ELISA kit, the optical density (OD) values of CK-MB and cTnT were measured at 450 nm, and their serum levels were calculated.

2.7 Cell Culture

Rat H9c2 cardiomyocytes were purchased from Procell Life Science & Technology Co., Ltd. (Wuhan, China). H9c2 cells in the logarithmic growth phase were resuspended at a density of 8×10^4 cells/mL, and 100 μL of the cell suspension was seeded into each well of a 96-well plate. The cells were cultured at 37°C with 5% CO_2 for 24 h until reaching 70% confluence. The cells were divided into blank, control, and hypoxia groups (2 h, 6 h, and 10 h). The culture medium was replaced with glucose-free Dulbecco's Modified Eagle Medium(DMEM) in all groups. Hypoxia groups were incubated in a hypoxia chamber (95% N_2, 5% CO_2) for the indicated durations, whereas the control group was cultured under normal conditions. After hypoxia treatment, the medium was discarded, and 100 μL of 10% CCK-8 solution was added to each well. Following incubation for 1.5 h, the absorbance was measured at 450 nm. Cell viability was calculated using the following formula: Cell viability (%) = [(Experimental group − Blank group) / (Control group − Blank group)] × 100%. A cell viability of 70%–80% was defined as the optimal hypoxia condition.

2.8. Screening of safe concentrations of active components

Blank, control, and 4 treatment groups were set up. Different concentration gradients were applied for each drug: FA, LIG, and SEA groups (0.25, 5, 50, 100, 200, 400, 800 μM), and the BOR group (1, 5, 25, 250, 500, 750, 1000 μM). After 24 h of treatment, cell viability was determined using the CCK-8 assay as described above to define the safe concentration range for each component.

2.9 Effects of active components on the viability of OGD-injured cells

Based on the safe concentration screening results, cells were divided into blank, control, model, and active component treatment groups (BOR/LIG/SEA: 0.5, 5, 50 μM; FA: 0.25, 1.25, 6.25 μM). When the cell confluence reached 70%, the cells were pretreated with a drug-containing medium for 24 hours. Subsequently, the model and treatment groups were replaced with glucose-free DMEM and incubated in an anaerobic chamber for 6 h, while the control group was maintained in a standard incubator. Cell viability was then measured using the CCK-8 assay as described above to evaluate the protective effects of the 4 active components on OGD-injured H9c2 cells.

2.10 Detection of Oxidative Stress and Cellular Injury Markers

H9c2 cells in the logarithmic growth phase were divided into a control group, a model group, and 4 drug-treated groups. After model establishment as described above, the supernatant was collected to measure LDH activity according to the kit instructions. Cells were harvested by scraping with phosphate-buffered saline (PBS), centrifuged (1000 rpm, 10 min, repeated twice), and homogenized by ultrasonication in an ice-water bath for 15 min. The levels of SOD and MDA were determined separately following the kit protocols.

2.11 Detection of Intracellular ROS Levels by DCFH-DA

H9c2 cells in the logarithmic growth phase were suspended at a density of 8×104 cells/mL, and 2 mL of the cell suspension was seeded into each well of a 6-well plate. Following the grouping and model establishment described above, the assay was performed strictly in accordance with the instructions of the ROS detection kit. Cells were incubated at 37°C in the dark for 30 min and washed 2–3 times with serum-free medium. Nuclei were stained with 4',6-diamidino-2-phenylindole (DAPI) at room temperature for 3–5 min, followed by another wash. Fluorescence images were captured using an inverted fluorescence microscope.

2.12 Selection of representative component

LIG was selected as a representative component of SJP for subsequent mechanistic studies, and 50 μM was identified as the most effective concentration based on the concentration-dependent protective effects observed (Figs. 3C–5).

2.13 Western Blotting

Western blot was performed to detect the phosphorylation levels of AKT/GSK3β pathway proteins and the expression of HIF-1α, to explore the mechanism of LIG. H9c2 cells were divided into a control group, a model group, and an LIG (50 μM) treatment group. After treatment, total protein was extracted, separated by SDS-PAGE, and transferred to membranes. The membranes were blocked with 5% skim milk at room temperature for 2 h. Primary antibodies were added and incubated overnight at 4°C: AKT (1:1000, SAB, 56093, 56 kDa), p-AKT (Ser473, 1:1000, SAB, 13357, 56 kDa), p-GSK3β (Ser9, 1:1000, Abclonal, AP0039, 46 kDa), GSK3β (1:1000, Abclonal, A11731, 46 kDa), HIF-1α (1:1000, Proteintech, 66730-1-Ig, 120 kDa), and GAPDH (1:1000, Proteintech, 60004-1-Ig, 36 kDa). After washing with Tris-buffered saline with Tween 20 (TBST), HRP-conjugated anti-rabbit/mouse secondary antibodies (1:10000, Bioss, bs-0295G/bs-0296G) were added and incubated at room temperature for 1 h. The bands were visualized by chemiluminescence and quantitatively analyzed using ImageJ software.

2.14 Mitochondrial Membrane Potential Detection (JC-1 Assay)

H9c2 cells in the logarithmic growth phase were suspended at a density of 8×10^4 cells/mL, and 100 μL of the cell suspension was seeded into each well of a 96-well plate. The cells were divided into a control group, a model group, and an LIG-treated group (50 μM). The assay was performed strictly in accordance with the kit instructions. The fluorescence intensities of red aggregates and green monomers were observed under a fluorescence microscope, and the red/green fluorescence ratio was calculated to evaluate the mitochondrial membrane potential.

2.15 Statistical Analysis

All data were analyzed using GraphPad Prism 10.1.2 software and expressed as Mean ± SD. The Student's t-test was used for comparisons between 2 groups. For multiple group comparisons, one-way analysis of variance (one-way ANOVA) was carried out, followed by Tukey's multiple comparisons test to discriminate between individual groups. In addition, Brown-Forsythe and Bartlett tests were performed to assess the homogeneity of variances. A value of $P < 0.05$ was considered statistically significant.

3. RESULTS

3.1 The protective effects of SJP on physiological status, cardiac function, and myocardial injury in mice with acute myocardial infarction

During the experiment, 2 mice in the MI group and one mouse in the SJP low-dose group died, leaving a total of 38 mice for statistical analysis. Compared with the sham-operated group, MI model mice exhibited mental depression, decreased activity, reduced food and water intake, lower body weight, and dry and rough hair (Fig. 1a). Echocardiography results showed that compared with the sham-operated group, the MI model group had significantly decreased left ventricular EF and FS, as well as significantly increased LVIDd and LVIDs, with statistical significance (Fig. 1b, c). Compared with the sham-operated group, the MI model group showed significantly increased heart weight and cardiac index (Fig. 1d). Serum levels of myocardial injury markers CK-MB, cTnT, and LDH were also significantly elevated (Fig. 1e, f).

Compared with the MI model group, mice in the SJP low-dose, high-dose, and captopril-positive control groups showed markedly improved mental status, activity, and food intake, reduced body weight loss, and smoother fur. Regarding cardiac function parameters, EF and FS were significantly increased, and left ventricular dilatation was reduced in all treatment groups. The SJP high-dose and captopril groups significantly reduced the elevated cardiac index, and the low-dose group also showed a decreasing trend in cardiac index. Serum myocardial injury marker levels were significantly decreased in all treatment groups. These results indicate that SJP improves general condition, inhibits pathological cardiac hypertrophy, enhances cardiac function, and alleviates myocardial injury in mice with acute myocardial infarction.

3.2. Effects of SJP on myocardial pathological morphology, fibrosis, and infarct size in mice with acute myocardial infarction

H&E staining revealed that the Sham group exhibited intact myocardial structure, neatly arranged myocardial fibers, and no obvious interstitial widening. In the MI group, the left ventricular cavity was enlarged, the ventricular wall was thinned, the myocardial structure was disrupted, fibers were disorganized, and marked inflammatory cell infiltration was observed. In all treatment groups, ventricular dilatation was attenuated, ventricular wall thickness was well preserved, myocardial fibers were arranged more regularly, the necrotic area was reduced, and inflammatory infiltration was alleviated (Fig. 2a). Masson staining showed minimal collagen deposition in the Sham group, whereas extensive collagen deposition and severe fibrosis were observed in the MI group; collagen deposition and fibrotic area were reduced in all treatment groups (Fig. 2b). TTC staining demonstrated uniform red staining in the Sham group, while a large pale necrotic area was present in the MI group; the necrotic area was significantly reduced, and the area of viable myocardium was increased in all treatment groups (Fig. 2c). Collectively, these results indicate that SJP can reduce myocardial pathological injury, reduce post-infarction fibrosis, decrease myocardial infarct size, and improve ventricular remodeling.

3.3 Protective effects of active components of SJP: OGD model establishment, safe concentration screening, and cytoprotective activity

To establish the OGD model, the effects of different OGD durations on the viability of H9c2 cells were examined. Cell viability decreased gradually with prolonged OGD, reaching approximately 70% after 6 h. Therefore, 6 h of OGD was selected to establish the injury model (Fig. 3A). Furthermore, the safe concentrations of BOR, FA, LIG, and SEA were screened using the CCK-8 assay. Cell viability remained > 90% at concentrations of BOR < 250 μM, FA < 5 μM, LIG < 200 μM, and SEA < 100 μM, indicating low cytotoxicity (Fig. 3B). Based on these results and pharmacokinetic data, the following concentrations were used in subsequent experiments: BOR, LIG, and SEA at 0.5, 5, and 50 μM; FA at 0.25, 1.25, and 6.25 μM. The viability of cells in the OGD model group was significantly reduced compared with the control group, confirming successful modeling. Compared with the model group, treatment with BOR (5 and 50 μM), FA (0.25, 1.25, and 6.25 μM), LIG (5 and 50 μM), and SEA (50 μM) significantly increased cell viability. These results indicate that the 4 active components effectively attenuate OGD-induced injury in cardiomyocytes (Fig. 3C)

3.4. Effects of active components of SJP on membrane damage and oxidative stress in OGD-injured H9c2 cells

After 6 h of OGD, compared with the control group, the activity of LDH in the supernatant of the model group was significantly increased, indicating cell membrane damage and LDH leakage. Meanwhile, intracellular MDA content and ROS levels were significantly elevated, while SOD activity was significantly decreased, indicating that OGD-induced lipid peroxidation damage and oxidative stress. Compared with the model group, treatment with 0.25, 1.25, and 6.25 μM FA, 0.5, 5, and 50 μM BOR and LIG, and 5 and 50 μM SEA significantly reduced LDH release, MDA content, and ROS levels, while increasing SOD activity (Figs. 4, 5), indicating that these effects repaired cell membrane damage, inhibited lipid peroxidation,

scavenged excess ROS, and enhanced antioxidant capacity. These results confirm that the 4 active components exert pronounced protective effects against OGD-induced injury in H9c2 cardiomyocytes.

3.5 Regulatory effect of ligustilide on the AKT/GSK3β/HIF-1α pathway in hypoxic H9c2 cells

Compared with the normoxic control group, the protein expression level of HIF-1α was significantly increased in hypoxic H9c2 cardiomyocytes, indicating that hypoxia successfully induced the upregulation of HIF-1α expression. Compared with the hypoxic model group, LIG intervention significantly increased the ratios of p-AKT/AKT and p-GSK3β/GSK3β, while markedly reducing the hypoxia-induced high expression of HIF-1α (Figs. 6a, b).

3.6. Effects of ligustilide on mitochondrial membrane potential

Compared with the control group, the JC-1 red/green fluorescence ratio was significantly decreased in the OGD model group, indicating that OGD injury induced a decline in mitochondrial membrane potential and impaired mitochondrial function in H9c2 cells. Compared with the model group, treatment with 50 μM LIG significantly increased the JC-1 red/green fluorescence ratio, effectively reversing the OGD-induced reduction in mitochondrial membrane potential, stabilizing mitochondrial function, and exerting a cardioprotective effect (Figs. 6c, d).

4. DISCUSSION

MI is associated with a high mortality rate and significant disability. The persistence of pathological responses, including myocardial oxidative stress disorder, mitochondrial damage, and cell apoptosis, after the onset of the condition, serves to exacerbate myocardial injury and ventricular remodelling. It is evident that current clinical interventions are inadequate in their capacity to entirely prevent continuous myocardial damage. SJP is a traditional Chinese patent medicine that is frequently employed for the treatment of myocardial ischemia. However, the precise active components and specific molecular mechanisms underlying its anti-MI effects remain to be elucidated. The present study systematically investigated the cardioprotective efficacy of SJP using in vivo and in vitro models. The effects of four major active components were verified, and the focus was placed on LIG to elucidate its mechanism of action from the perspective of mitochondrial function and the AKT/GSK3β/HIF-1α pathway.

MI has been shown to induce myocardial necrosis, leading to decreased ventricular systolic function, pathological ventricular dilation, abnormal release of myocardial injury markers, disordered myocardial structure, and fibrotic remodelling. These are core pathological features of progressive cardiac dysfunction.[16] The present study corroborates earlier findings by demonstrating that SJP significantly increases EF and FS in mice with MI, improves ventricular systolic function, and inhibits ventricular dilation. Concurrently, SJP effectively reduced serum levels of myocardial injury markers, including CK-

MB, cTnT, and LDH, thereby alleviating myocardial necrosis. Furthermore, H&E, Masson, and TTC staining revealed that SJP normalised myocardial fibre arrangement, inhibited inflammatory infiltration and myocardial fibrosis, and reduced infarct size. This effect was dose-dependent, with optimal efficacy observed at high doses. These findings systematically confirm the overall cardioprotective effect of SJP against MI.

Early myocardial ischemia is frequently accompanied by mitochondrial dysfunction and excessive activation of oxidative stress, which are pivotal processes contributing to cardiomyocyte injury and cardiac dysfunction. [17] Myocardial hypoxia leads to significant accumulation of ROS, triggering lipid peroxidation and reducing SOD activity, ultimately exacerbating cardiomyocyte injury.[18] In this study, the utilisation of an OGD model in H9c2 cardiomyocytes revealed that BOR, FA, LIG, and SEA significantly enhanced cell viability, reduced LDH release, decreased MDA and ROS levels, and increased SOD activity. The results of this study demonstrate that SJP exerts cardioprotective effects by antagonising oxidative stress through multiple active components in a synergistic manner.

Mitochondria are vital organelles that facilitate energy metabolism and ensure the survival of cardiomyocytes. Ischemia and hypoxia have been demonstrated to induce a decline in mitochondrial membrane potential and dysfunction, thereby exacerbating oxidative stress and apoptotic injury. [19] As a key active component of SJP, LIG significantly reversed the reduction in mitochondrial membrane potential induced by OGD, whilst also maintaining mitochondrial structural and functional stability, and inhibiting mitochondria-mediated cell injury. AKT (protein kinase B) is a core kinase that regulates cell survival, proliferation, and metabolism.[20] Glycogen synthase kinase 3β (GSK3β) has been identified as a key downstream negative regulator of AKT. Phosphorylation and activation of AKT inhibit GSK3β activity via phosphorylation, thereby promoting cell survival and suppressing apoptosis.[21] Hypoxia-inducible factor-1α (HIF-1α) is a master transcription factor that functions under conditions of hypoxia. Aberrant expression of this factor has been demonstrated to intensify myocardial inflammation and injury under hypoxic conditions.[22] Furthermore, LIG activated the AKT/GSK3β signalling pathway, resulting in increased AKT and GSK3β phosphorylation levels, and decreased HIF-1α expression. The AKT/GSK3β pathway has been identified as a critical regulator of cell survival, energy metabolism and anti-apoptosis .[23] Furthermore, moderate inhibition of excessive HIF-1α expression has been shown to alleviate secondary injury induced by hypoxic stress.[24] The findings suggest that LIG exerts cardioprotective effects by stabilising mitochondrial function and modulating the AKT/GSK3β/HIF-1α pathway.

The present study corroborated the notion that boron, folic acid, L-carnitine and selenium have cardioprotective properties, and L-carnitine was selected for in-depth mechanistic investigation with solid scientific rationale. A component content analysis revealed that LIG is the core phthalide active constituent of Rhizoma Chuanxiong, the monarch herb of SJP, with a high abundance in both the formulation and raw medicinal materials, serving as the primary material basis for its pharmacological effects.Pharmacokinetic and tissue distribution studies further verified that LIG rapidly targets and accumulates in myocardial tissue. Despite its predominant existence as metabolic derivatives in the

blood, it exerts a stable effect on the heart and directly contributes to myocardial injury repair, thus establishing itself as a pivotal component responsible for the rapid onset of SJP. [25] In consideration of the in vitro outcomes of the present study, LIG demonstrates notable efficacy in enhancing myocardial oxidative stress and rectifying mitochondrial impairment. Given its high content, cardiac-targeted distribution, and potent in vitro efficacy, LIG has been identified as the core active component of SJP against acute myocardial infarction (AMI). In comparison with single chemical drugs, SJP, which is characterised by multi-component and multi-target actions, has been shown to synergistically regulate multiple pathological injuries in MI. This is in alignment with the complex pathogenesis of MI, and it has been demonstrated to offer unique advantages in traditional Chinese medicine applications. [26]

This study has certain limitations. First, only 4 major active components were screened, and the potential effects of other minor components were not comprehensively investigated. Second, the upstream mechanism by which SJP regulates the AKT/GSK3β/HIF-1α pathway remains to be further explored, and pathway-specific inhibitors were not used to validate its causal role in ligustilide-mediated cardioprotection. Third, echocardiographic and histopathological assessments were not performed under blinded conditions, which may have introduced potential detection bias. Finally, the experimental conclusions are mainly derived from animal and cell models, requiring further validation in clinical studies.

5. CONCLUSION

The present study systematically elucidated the pharmacological effects and mechanisms of SJP and its active components against myocardial ischemic injury at the in vivo, cellular, and molecular levels. In vivo results confirmed that SJP significantly improved cardiac function in mice with acute myocardial infarction, reduced serum levels of myocardial injury markers, alleviated myocardial pathological damage and fibrosis, and effectively reduced myocardial infarct size, exerting a definite cardioprotective effect. In vitro experiments further verified that the presence of boron, fluorine, ligation, and sulfonation in SJP could effectively alleviate OGD-induced injury in H9c2 cardiomyocytes, enhance cell viability, reduce LDH release, inhibit oxidative stress, and improve cellular antioxidant capacity, providing a material basis for the cardioprotective effect of SJP. Mechanistic studies demonstrated that the key active component LIG reversed the OGD-induced decrease in mitochondrial membrane potential and stabilized mitochondrial function. Furthermore, LIG regulated cell survival and inhibited oxidative stress by activating the AKT/GSK3β signalling pathway and downregulating the expression of HIF-1α, ultimately attenuating myocardial ischemic injury. In conclusion, SJP exhibits significant activity against myocardial ischemic injury, and its effects are closely associated with ligustilide-mediated activation of the AKT/GSK3β/HIF-1α pathway and stabilization of mitochondrial function.

Declarations

The authors report no conflicts of interest.

Funding Statement:

This study was supported by the Natural Science Foundation of Tianjin (No. 25JCLZJC0022) and the Special Project of Modern Traditional Chinese Medicine New Quality Productivity Science and Technology Innovation Project (No. 24ZXZKSY00010).

Author Contribution

Yue Weng and Xinyu He performed the research. Xueke Liu and Peishuang Yu designed the research study. Yanyan Xu and Shenshen Yan contributed essential reagents or tools. Peishuang Yu and Yujie Gong analyzed the data. Yue Weng and Xinyu He wrote the paper.

Data Availability

Data availability statementThe data supporting the findings of this study are not publicly available due to privacy/ethical restrictions. They are available from the corresponding author upon reasonable request.

References

1. Saha, T., & Soliman-Aboumarie, H. (2025). Review of Current Management of Myocardial Infarction[J]. *Journal of Clinical Medicine*, *14*(17), 6241. https://doi.org/10.3390/jcm14176241
2. Li, Z., Hou, J., Deng, Y., Zhi, H., Wu, W., Yan, B., Chen, T., Tu, J., Zhu, Z., Wu, W., & Guo, D. (2020). Exploring the protective effects of Danqi Tongmai tablet on acute myocardial ischemia rats by comprehensive metabolomics profiling. *Phytomedicine*, *74*, 152918. https://doi.org/10.1016/j.phymed.2019.152918
3. Ramya, V., Shyam, K. P., Kowsalya, E., Balavigneswaran, C. K., & Kadalmani, B. (2022). Dual roles of coconut oil and its major component lauric acid on redox nexus: focus on cytoprotection and cancer cell death. *Front Neurosci*, *16*, 833630. https://doi.org/10.3389/fnins.2022.833630
4. Welt, F. G. P., Batchelor, W., Spears, J. R., et al. (2024). Reperfusion injury in patients with acute myocardial infarction: JACC scientific statement[J]. *Journal of the American College of Cardiology*, *83*(22), 2196–2213. https://doi.org/10.1016/j.jacc.2024.02.056
5. Le, W., Liao, J., Zhang, Y., et al. (2025). Integrated metabolomics and the microbiome reveal the compatibility mechanism of the Suxiao Jiuxin pill in the treatment of stable coronary artery disease[J]. *Chinese Medicine*, *20*(1), 140. https://doi.org/10.1186/s13020-025-01198-8
6. Ruan, X., Li, Y., Sun, Y., et al. (2021). Efficacy and safety of Suxiao Jiuxin Pill in the treatment of stable angina (Qi stagnation and blood stasis syndrome): study protocol of a randomized, double-blind, placebo-controlled, multi-center clinical trial. *Trials*, *22*(1), 466. https://doi.org/10.1186/s13063-021-05448-6

7. Hu, Y., Wang, Y., Wang, S., et al. (2024). Efficacy and Safety of Suxiao Jiuxin Pills in the Treatment of Chronic Coronary Syndrome with Intolerance to Adverse Effects of Long-acting Nitrates: A Multicenter, Randomized, Double-blind, Placebo-controlled Study[J]. *BMC Complementary Medicine and Therapies*, *24*(1), 356. https://doi.org/10.1186/s12906-024-04661-5
8. Liu, J., Lei, Z., Wang, Z., et al. (2025). Ethnobotanical usages, phytochemistry, pharmacology, and quality control of chuanxiong rhizoma: A review. *J Ethnopharmacol*, *337*(Pt 3), 118902. https://doi.org/10.1016/j.jep.2024.118902
9. Wu, Q., Mao, Z., Liu, J., et al. (2020). Ligustilide attenuates ischemia reperfusion-induced hippocampal neuronal apoptosis via activating the PI3K/Akt pathway[J]. *Frontiers In Pharmacology*, *11*(6). https://doi.org/10.3389/fphar.2020.00979
10. Cao, Y., Dong, Z., Yang, D., et al. (2021). Alleviation of glucolipotoxicity-incurred cardiomyocyte dysfunction by Z-ligustilide involves in the suppression of oxidative insult, inflammation, and fibrosis[J]. *Chemistry And Physics Of Lipids*, *241*(11), 105138–105138. https://doi.org/10.1016/j.chemphyslip.2021.105138
11. Zhang, K., Luan, G., Zhang, J., et al. (2025). Ligustilide covalently binds to Cys254 of the creatine kinase, M-type protein, ameliorating acute myocardial ischemia by enhancing the creatine phosphate level[J]. *Phytomedicine*, *139*, 156532. https://doi.org/10.1016/j.phymed.2025.156532
12. Ruan, X., Chen, T., Wang, X., et al. (2017). Suxiao Jiuxin Pill protects cardiomyocytes against mitochondrial injury and alters gene expression during ischemic injury[J]. *Experimental & Therapeutic Medicine*, *14*(4), 3523–3532. https://doi.org/10.3892/etm.2017.4964
13. Wu, Q., Liu, J., Tian, L. Y., & Wang, N. (2022). [Mitophagy mediated by ligustilide relieves OGD/R-induced injury in HT22 cells]. Zhongguo Zhong Yao Za Zhi. *China Journal of Chinese Materia Medica*, *47*, 1897–1903. https://doi.org/10.19540/j.cnki.cjcmm.20211029.404
14. Shang, Y., Zhu, Y., Zhou, S., et al. (2025). A UPLC-MS/MS coupled with GC-MS method for quantification of twenty-one chemical ingredients from Suxiao Jiuxin pill in multiple tissue of rat and its application to tissue distribution study[J]. *Journal of Pharmaceutical and Biomedical Analysis*, *252*, 116461. https://doi.org/10.1016/j.jpba.2024.116461
15. Zhou, Q., Huang, W., Xiong, J., et al. (2023). CDCA8 promotes bladder cancer survival by stabilizing HIF1α expression under hypoxia[J]. *Cell Death & Disease*, *14*(10), 658. https://doi.org/10.1038/s41419-023-06189-x
16. Tan, D., Lye, Y. E., Patel, P., et al. (2026). Beyond Reperfusion: Early Molecular Drivers and Therapeutic Opportunities in Acute Post-Infarction Cardiac Fibrosis[J]. *International Journal of Molecular Sciences*, *27*(10), 4409. https://doi.org/10.3390/ijms27104409
17. Juricic, S., Klac, J., Stojkovic, S., et al. (2026). Molecular and Cellular Mechanisms of Myocardial Ischemia and Reperfusion Injury. *A Narrative Review[J] Cells*, *15*(3), 265. https://doi.org/10.3390/cells15030265
18. Zhang, Y., Jiang, M., & Wang, T. (2024). Reactive oxygen species (ROS)-responsive biomaterials for treating myocardial ischemia-reperfusion injury[J]. *Frontiers in bioengineering and biotechnology*, *12*,

1469393. https://doi.org/10.3389/fbioe.2024.1469393

19. Ma, R., Lu, D., Yang, Z., et al. (2025). Emerging therapy strategies for energy metabolism in acute myocardial infarction[J]. *Journal of Translational Medicine*, *23*(1), 1140. https://doi.org/10.1186/s12967-025-07088-9
20. Minegishi, K., Dobashi, Y., Kimura, E., et al. (2025). AKT: A Central Node in Complex Signaling Cascades[J]. *Frontiers in Bioscience-Landmark*, *30*(6), 26414. https://doi.org/10.31083/FBL26414
21. Ajzashokouhi, A. H., Rezaee, R., Omidkhoda, N., et al. (2023). Natural compounds regulate the PI3K/Akt/GSK3β pathway in myocardial ischemia-reperfusion injury[J]. *Cell Cycle*, *22*(7), 741–757. https://doi.org/10.1080/15384101.2022.2161959
22. Watanabe, M., Ikeda, M., Abe, K., et al. (2025). Excessive HIF-1α driven by phospholipid metabolism causes septic cardiomyopathy through cytopathic hypoxia[J]. *Nature Cardiovascular Research*, *4*(9), 1077–1093. https://doi.org/10.1038/s44161-025-00687-1
23. Ren, Z., Zhong, H., Song, C., et al. (2020). Insulin promotes mitochondrial respiration and survival through PI3K/AKT/GSK3 pathway in human embryonic stem cells[J]. *Stem cell reports*, *15*(6), 1362–1376. https://doi.org/10.1016/j.stemcr.2020.10.008
24. Xu, X., Yang, M., Zhang, B., et al. (2023). HIF-1α participates in secondary brain injury through regulating neuroinflammation[J]. *Translational Neuroscience*, *14*(1), 20220272. https://doi.org/10.1515/tnsci-2022-0272
25. Shang, Y., Ge, M., Zhao, P., et al. (2024). A pharmacokinetic study on twenty-one compounds in rat plasma by integrating UPLC-QQQ-MS/MS with GC-MS after oral administration of Suxiao Jiuxin pill[J]. *Arabian Journal of Chemistry*, *17*(1), 105397. https://doi.org/10.1016/j.arabjc.2023.105397
26. Hu, X., Liu, Y., Francis, O. B., et al. (2025). Efficacy, safety, and pharmacological mechanism of Suxiao Jiuxin Pill in acute coronary syndrome: A systematic review and network pharmacology analysis[J]. *European Journal of Integrative Medicine*, *78*, 102524. https://doi.org/10.1016/j.eujim.2025.102524

Figures

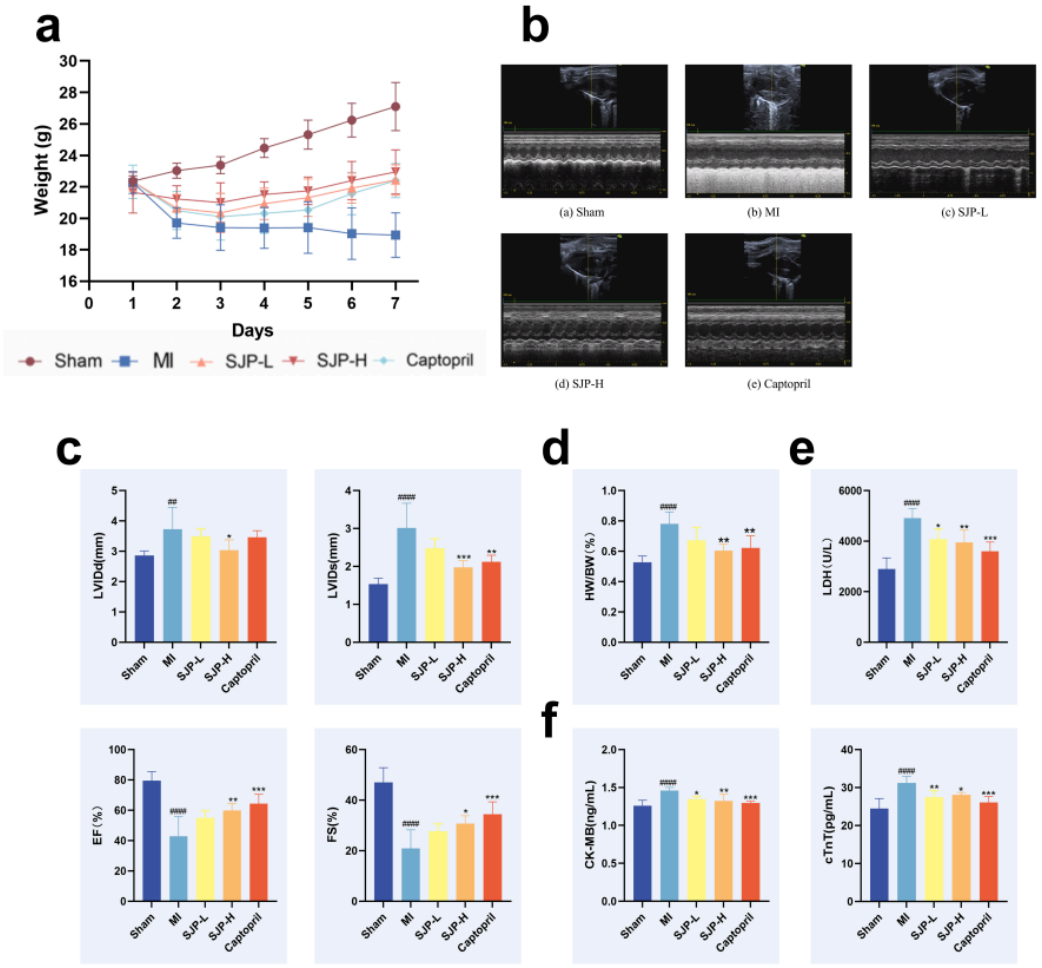


Figure 1

Effects of SJP on general status, body weight, and cardiac function in mice with acute myocardial infarction (n=6). **a**.Body weight changes of mice in each group over 7 days. **b**. Representative M-mode echocardiographic images of the left ventricle in different groups. **c** Echocardiographic parameters of LVIDd, LVIDs, EF, and FS.**d**. Heart weight/body weight ratio (HW/BW).**e–g**: LDH, CK-MB, and cTnT. (#P < 0.05, ## P < 0.01, ### P < 0.001, #### P < 0.0001 vs. Sham group; * P < 0.05, ** P < 0.01, *** P < 0.001 vs. MI group.)Data are presented as mean ± SD (n = 6 per group)

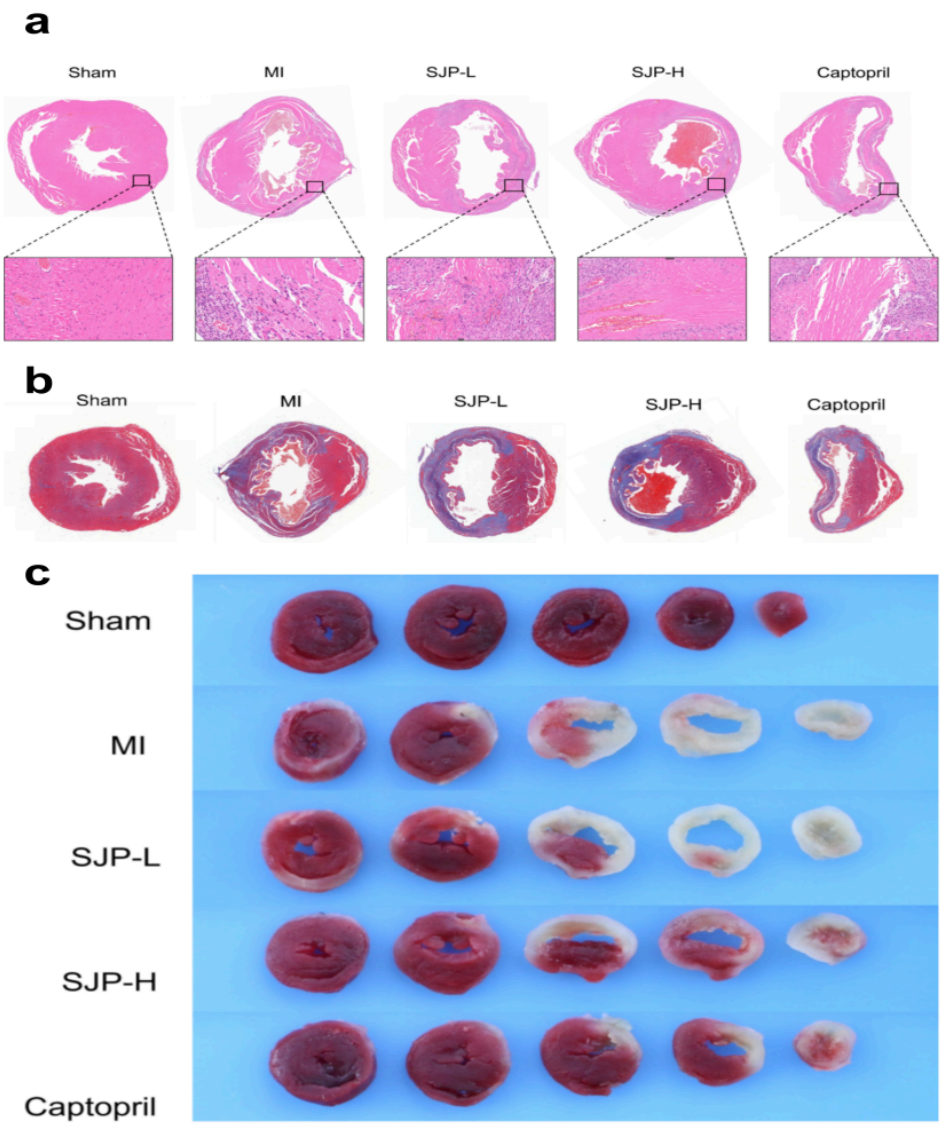


Figure 2

Effects of SJP on myocardial pathological morphology, fibrosis, and infarct size in mice with acute myocardial infarction. **a**. HE staining results; **b**. Masson staining results; **c**. TTC staining results

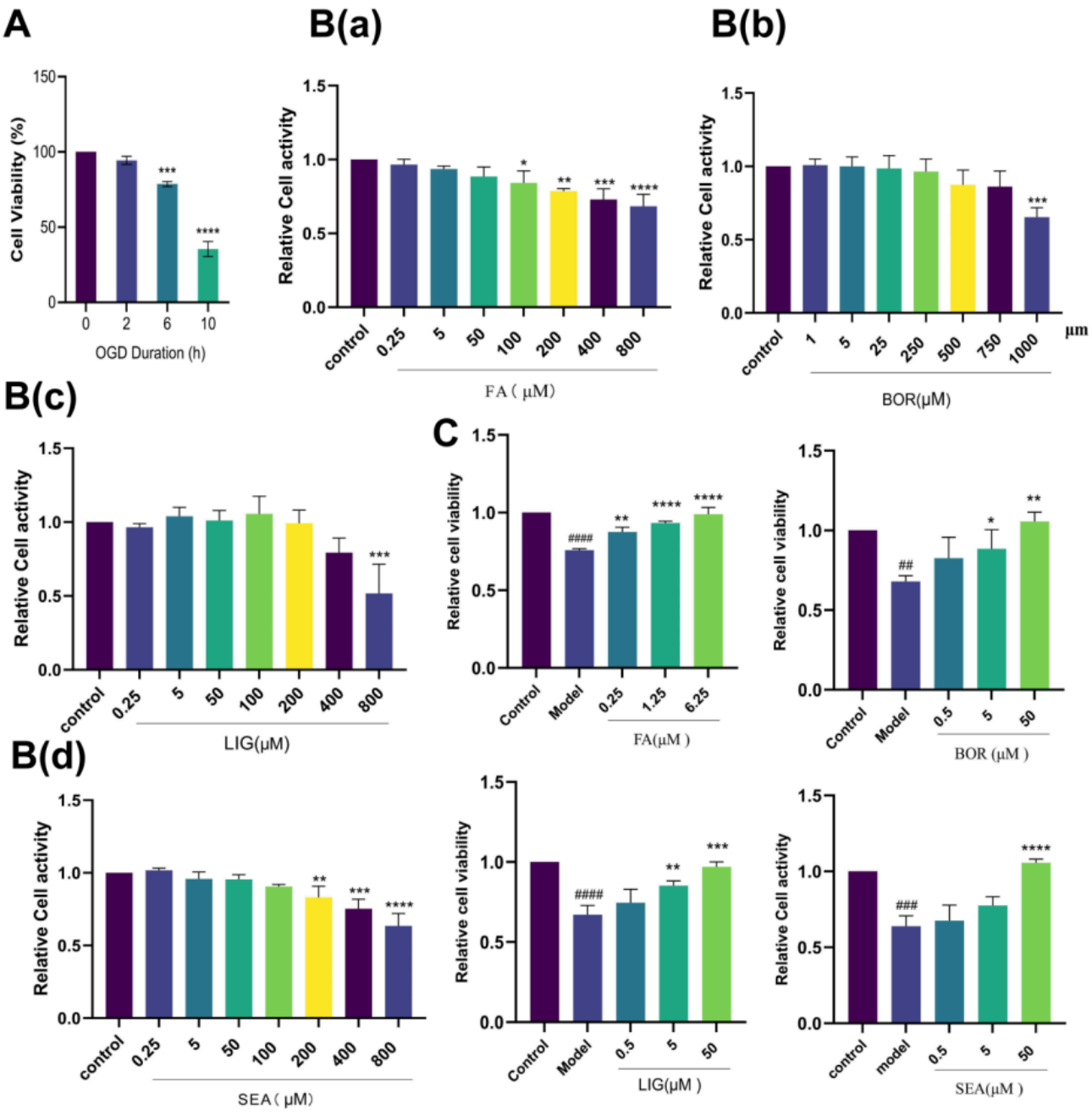


Figure 3

Effects of active components of SJP: OGD model establishment, safe concentration screening, and cytoprotective activity. (n = 3) **A.** Effects of different OGD durations on the viability of H9c2 cardiomyocytes;(*** P < 0.001 ,****P < 0.0001vs. control group.) **B.**Cytotoxicity and safe concentration screening of different concentrations of BOR, FA, LIG, and SEA in H9c2 cardiomyocytes;(* P < 0.05, ** P < 0.01, *** P < 0.001,****P < 0.0001vs. control group.) **C**. Effects of BOR, FA, LIG, and SEA at safe

concentrations on the viability of H9c2 cardiomyocytes after OGD injury.(## P < 0.01, ### P < 0.001, #### P < 0.0001 vs. control group; * P < 0.05, ** P < 0.01, *** P < 0.001,**** P < 0.0001 vs. model group.) Data were presented as mean ± SD (n = 3, three independent experiments).

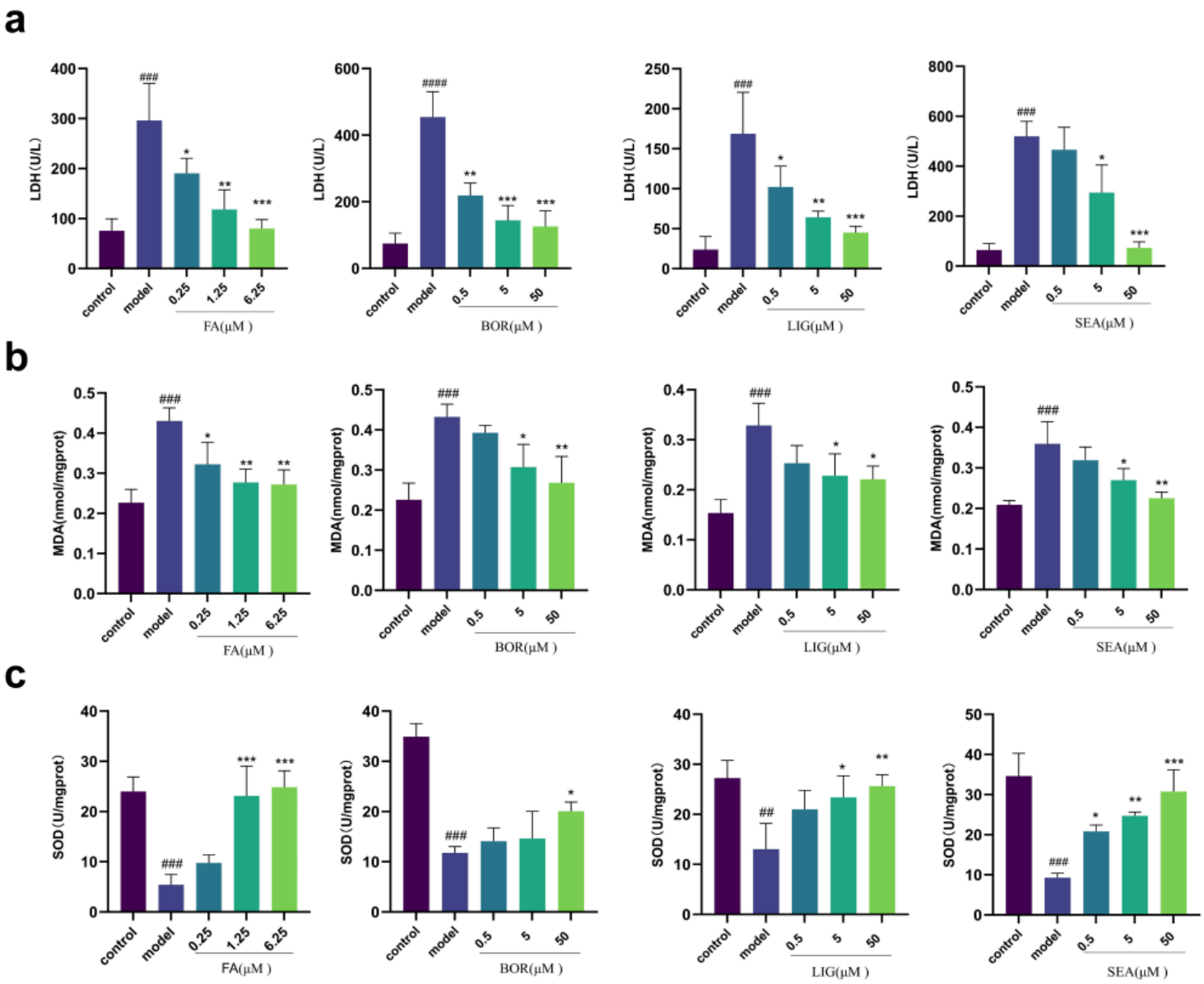


Figure 4

Effects of active components of SJP on LDH release, MDA content, and SOD activity in oxygen-glucose deprivation (OGD)-injured H9c2 cardiomyocytes. (n=3) **a**. Effects of active components of SJP on LDH activity in the supernatant of OGD-injured H9c2 cells; **b.** Effects of active components of SJP on intracellular MDA content in OGD-injured H9c2 cells; **c**. Effects of active components of SJP on intracellular SOD activity in OGD-injured H9c2 cells.(## P < 0.01, ### P < 0.001, #### P < 0.0001 vs.

control group; * P < 0.05, ** P < 0.01, *** P < 0.001 vs. model group.)Data were presented as mean ± SD (n = 3, three independent experiments)

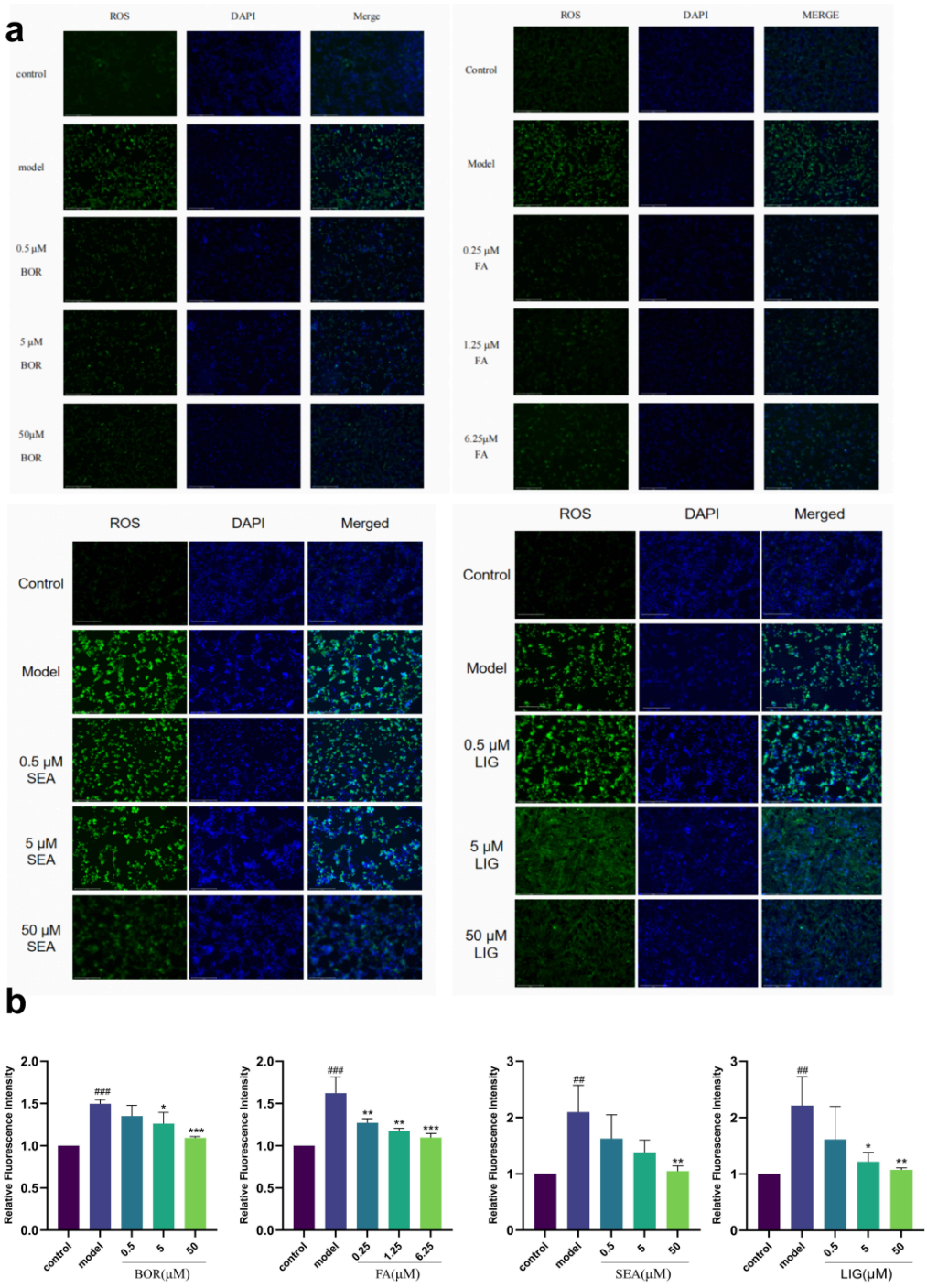


Figure 5

Effects of active components of SJP on intracellular ROS levels in OGD-injured H9c2 cells. (n=3) **a**. Representative fluorescence microscopy images of intracellular ROS (green) and DAPI (blue) staining in

H9c2 cardiomyocytes.**b**. Quantitative analysis of relative ROS fluorescence intensity in H9c2 cardiomyocytes.(## P < 0.01, ### P < 0.001 vs. control group; * P < 0.05, ** P < 0.01, *** P < 0.001 vs. model group.) Data were presented as mean ± SD (n = 3, three independent experiments)

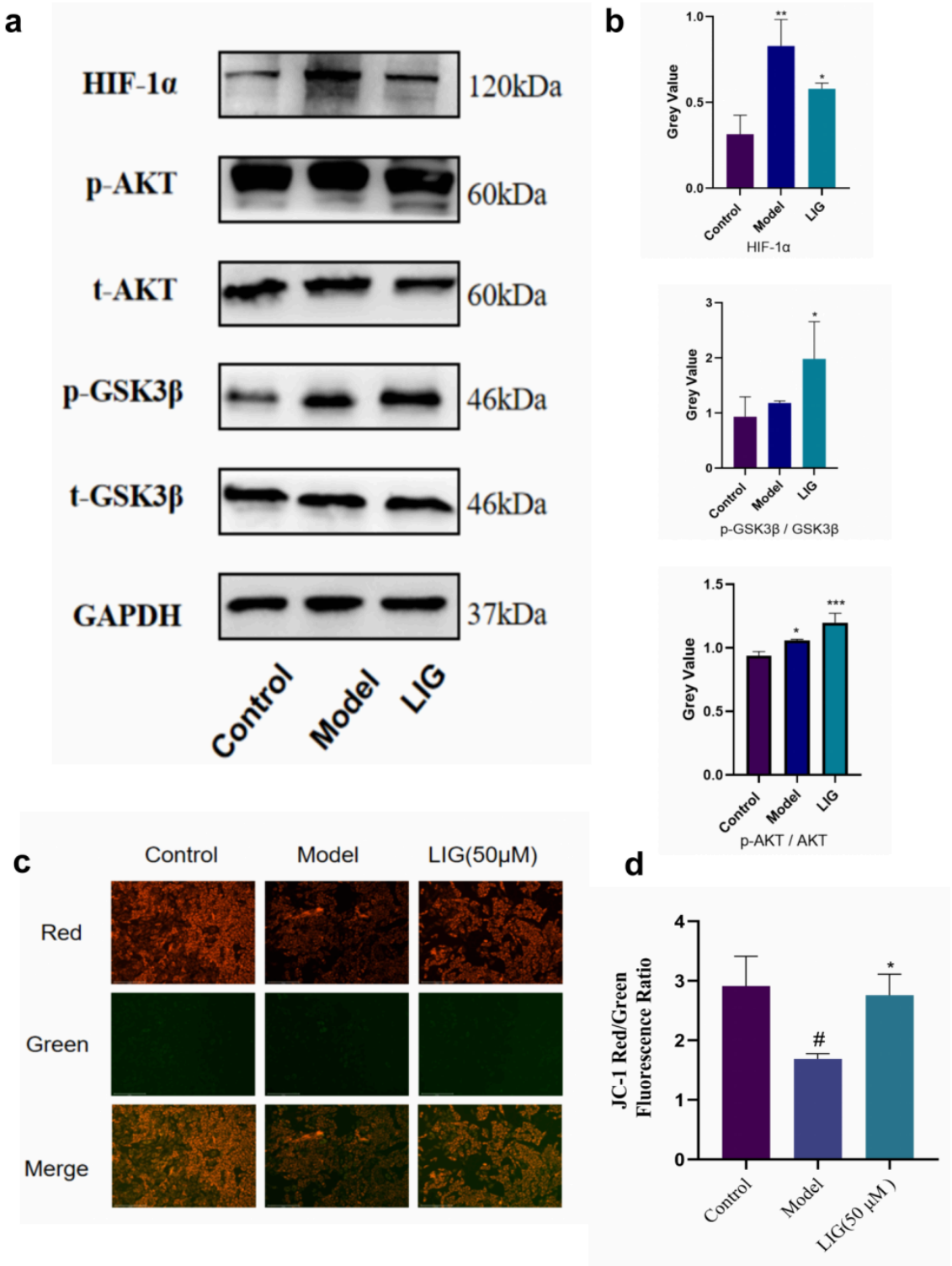


Figure 6

LIG regulates signaling pathways and improves mitochondrial function in hypoxic cardiomyocytes. (n=3) **a**. Representative Western blot bands showing LIG-mediated regulation of the Akt/GSK-3β/HIF-1α pathway in OGD-injured H9c2 cardiomyocytes. **b**. Densitometric analysis of p-Akt/Akt, p-GSK-3β/GSK-3β ratios, and HIF-1α expression in OGD-injured H9c2 cardiomyocytes treated with LIG.(* $P < 0.05$, ** $P < 0.01$, *** $P < 0.001$ vs. control group.) **c**. Effects of LIG on mitochondrial membrane potential in OGD-injured H9c2 cells (JC-1 fluorescence staining). **d**. Quantitative analysis of mitochondrial membrane potential in OGD-injured H9c2 cells treated with LIG.(# $P < 0.05$ vs. control group; * $P < 0.05$ vs. model group.) Data were presented as mean ± SD (n = 3, three independent experiments)

Supplementary Files

This is a list of supplementary files associated with this preprint. Click to download.

- image1.png